Title
Regulatory T cells in skin are uniquely poised to suppress profibrotic immune responses

Journal
Science Immunology, 4(39)

ISSN
2470-9468

Authors
Kalekar, Lokesh A
Cohen, Jarish N
Prevel, Nicolas
et al.

Publication Date
2019-09-13

DOI
10.1126/sciimmunol.aaw2910

Peer reviewed

Published in final edited form as:

Sci Immunol. 2019 September 06; 4(39): . doi:10.1126/sciimmunol.aaw2910.

Regulatory T Cells in Skin are Uniquely Poised to Suppress Profibrotic Immune Responses

Lokesh A. Kalekar[1], **Jarish N. Cohen**[1], **Nicolas Prevel**[1], **Priscila Muñoz Sandoval**[1], **Anubhav Mathur**[1], **Joshua M. Moreau**[1], **Margaret Lowe**[1], **Audrey Nosbaum**[2], **Paul J. Wolters**[3], **Anna Haemel**[1], **Francesco Boin**[4], **Michael D. Rosenblum**[1]

[1]Department of Dermatology, University of California, San Francisco, USA

[2]Department of Allergy and Clinical Immunology, Centre Hospitalier Lyon-Sud, Hospices Civils de Lyon, France

[3]Department of Medicine, University of California, San Francisco, USA

[4]Department of Rheumatology, University of California, San Francisco, USA

Abstract

At the center of fibrosing diseases is the aberrant activation of tissue fibroblasts. The cellular and molecular mechanisms of how the immune system augments fibroblast activation have been described; however, little is known about how the immune system controls fibroblast function in tissues. Here, we identify regulatory T cells (Tregs) as important regulators of fibroblast activation in skin. Bulk cell and single cell analysis of Tregs in murine skin and lungs revealed that Tregs in skin are transcriptionally distinct and skewed towards T_H2 differentiation. When compared to Tregs in lung, skin Tregs preferentially expressed high levels of GATA3, the master T_H2 transcription factor. Genes regulated by GATA3 were highly enriched in skin 'T_H2 Treg' subsets. In functional experiments, Treg depletion resulted in a preferential increase in T_H2 cytokine production in skin. Both acute depletion and chronic reduction of Tregs resulted in spontaneous skin fibroblast activation, profibrotic gene expression and dermal fibrosis, all of which were exacerbated in a bleomycin-induced murine model of skin sclerosis. Lineage-specific deletion of *Gata3* in Tregs resulted in an exacerbation of T_H2 cytokine secretion that was preferential to skin, resulting in enhanced fibroblast activation and dermal fibrosis. Taken together, we demonstrate that Tregs play a critical role in regulating fibroblast activation in skin and do so by expressing a unique tissue-restricted transcriptional program that is mediated, at least in part, by GATA3.

Address of Correspondence: Michael D. Rosenblum M.D., Ph.D., Medical Sciences Building, Health Sciences West - 1201B, 513 Parnassus Avenue, San Francisco, CA 94132, Ph: 415-476-1685, Michael.Rosenblum@ucsf.edu.

AUTHOR CONTRIBUTIONS

M.D.R conceived the project and directed research. M.D.R and L.A.K designed the study and wrote the manuscript. L.A.K performed the experiments, collected and analyzed the data. J.N.C, N.P, P.M.S, A.M, J.M.M., M.L., and A.N., assisted with experiments and data generation. P.J.W., A.H., and F.B., provided research input.

COMPETING INTERESTS

M.D.R. is the founder of TRex Bio, a co-founder of Sitryx, and a consultant with Celgene. The other authors declare that they have no competing interests.

DATA AND MATERIALS AVAILABILITY

RNA-seq data have been deposited in the National Center for Biotechnology Information's Gene Expression Omnibus and are available under accession number GSE xref. All other data needed to evaluate the conclusions of the paper are present in the paper or the Supplementary Materials.

INTRODUCTION

Fibroblast activation is a key event in tissue remodeling after injury. However, excessive deposition of extracellular matrix (ECM) components by activated fibroblasts leads to tissue fibrosis, a hallmark of several life-threatening diseases, including systemic sclerosis, idiopathic pulmonary fibrosis and end-stage liver disease (1). It is becoming increasingly evident that the immune system plays a major role in the activation of quiescent fibroblasts to ECM-producing myofibroblasts (2). Effector T cell production of the T_H2 cytokines, IL-4 and IL-13, drives fibroblast activation *via* signaling through their cognate receptors expressed on fibroblasts and/or on tissue myeloid cells, resulting in increased ECM deposition (3–5). Expression of TGF-β by multiple immune and non-immune cell types directly induces myofibroblast differentiation and drives the progression of tissue fibrosis (6).

A major function of the immune system is to regulate inflammation in tissues. Defined populations of regulatory cells reside in non-lymphoid organs and act to mitigate tissue damage, both in the steady state and after injury. Regulatory T cells (Tregs) are the best characterized regulatory cell subset and are defined by the expression of the X-linked transcription factor FoxP3 (7, 8). Tregs have a predilection to stably reside in barrier organs such as the gastrointestinal tract, lungs and skin (7–11). In these locations, they utilize unique tissue-restricted mechanisms to control inflammatory responses (12). In addition, these Tregs play major roles in mediating tissue-specific functions, such as muscle regeneration (13), lipid and glucose metabolism (14), hair follicle cycling (11) and epidermal repair (15).

While the mechanisms by which the immune system activates fibroblasts have been extensively studied, it is currently unknown whether the regulatory arm of the immune system can control these cells and play a role in attenuating tissue fibrosis. Furthermore, whether these mechanisms differ in specific tissues remains to be elucidated. Tregs have been shown to secrete the pro-fibrotic cytokine, TGF-β (6); however, these cells are also capable of suppressing the production of profibrogenic cytokines, such as IL-4 and IL-13 (16). These mechanisms appear to be both tissue and context dependent (17–20). Thus, despite our increasing understanding of how Tregs function, it is currently unclear as to whether the net effect of these cells is to augment or attenuate tissue fibrosis. Additionally, it is currently unclear how tissue-specific transcriptomes in Tregs inform fibrosis biology. In the current study, we show that Tregs in skin are uniquely differentiated to attenuate dermal fibroblast activation and skin fibrosis.

RESULTS

Single cell transcriptional analysis of Tregs in murine skin reveals a predominance of “Type 2” Tregs

It is becoming increasingly appreciated that tissue-resident Tregs are comprised of multiple subsets that have unique mechanisms of action that largely depend on the tissues in which they reside (12). To begin to better understand the functional heterogeneity of Tregs in skin,

we performed bulk cell and single cell RNA sequencing (RNAseq) of Tregs isolated from murine skin during the telogen phase of the hair follicle cycle (11). For bulk cell analysis, we performed whole transcriptome RNAseq on live $CD45^+CD3^+CD4^+CD25^+Foxp3\text{-}GFP^+$ cells that were sort purified from skin and skin-draining lymph nodes (SDLNs) of Foxp3-GFP reporter mice (21). Differential gene expression analysis of Tregs in skin vs. Tregs in SDLNs revealed that Tregs in skin express relatively high levels of T_H2-associated genes (Figure 1A). Genes associated with T_H2 differentiation that were highly expressed in skin Tregs include the master T_H2 transcription factor, *Gata3* (22) and the T_H2-associated transcription factor, *Irf4* (23) (Figure 1A). Ingenuity Pathway Analysis™ revealed that Tregs in skin express significantly higher levels of genes associated with T_H2 differentiation when compared to Tregs in SDLNs (Ratio = 40/150; 0.267), with a z-score of 1.616 (indicating activation of the pathway) and a Benjamini-Hochberg FDR corrected P-value of 5.74×10^{-14} (Figure 1B). Gene set enrichment analysis (24) (25) revealed that a significant number of genes differentially expressed in skin Tregs vs. SDLNs Tregs are regulated by GATA3 (26), with a p-value of <0.0001 and false discovery rate of <0.0001 (Figure 1C, Table S1). In an attempt to elucidate whether T_H2-associated genes were expressed by all Tregs in skin or restricted to a specific subset, we sort purified Tregs from murine skin (using the same strategy as outlined above) and performed single cell RNAseq using the 10xGenomics platform (27). Data displayed as a dimensionally reduced t-SNE (t-distributed stochastic neighbor embedding) plot revealed skin Tregs clustering in 7 transcriptionally distinct subsets (Figure 1D). A heatmap of the top 5 differentially expressed genes defining each cluster is shown in Figure 1E. Interestingly, high levels of *Gata3* expression were observed across all subsets (Figure 1F). In contrast, transcription factors that define other T_H subsets, such as *Rorc* (T_H17; (28)) and *Tbx21* (T_H1; (29)) were not expressed at appreciable levels in any of the skin Treg clusters (Figure 1F). The T_H2-associated transcription factor *Irf4* was observed to be differentially expressed between Tregs in skin and Tregs in SDLNs at the bulk cell 'population' level (Figure 1A) showed a similar expression pattern to *Gata3* at the single cell level. However, *Irf4* expression was detected in fewer cells when compared to *Gata3* at the single cell level (Figure 1F). Genes known to be regulated by GATA3 (i.e. *Fos, Il1rl1, Ero1l, Maf, Nfkbiz*) (26) showed similar levels of expression and a similar expression pattern across skin Treg clusters when compared to *Gata3* (Figure 1F, G). Interestingly, *Areg* (amphiregulin), a gene shown to be regulated by GATA3 and involved in imparting Tregs with the capacity for tissue repair (30), was one the top 5 genes defining cluster 3 (Figure 1E).

To determine if Tregs in skin are "T_H2 skewed" relative to Tregs in other barrier tissues, we performed single cell RNAseq on Tregs isolated from healthy lungs of Foxp3-GFP mice and compared the transcriptome of these cells to Tregs isolated from skin. Lung Tregs clustered in 6 transcriptionally distinct subsets (Supplementary Figure 1A) and relatively diffusely expressed Treg related genes such as *Il2ra* and *Ctla4* (Supplementary Figure 1B). *Gata3* expression in lung Tregs was fairly diffuse, while *Rorc*, *Tbx21* and *Irf4* were not detected at appreciable levels (Supplementary Figure 1B). Quantification of GATA3-regulated genes in lung Tregs revealed minimal expression of *Areg*, Il1rl1, and *Ero1l*; whereas *Fos*, *Maf* and *Nfkbiz* were expressed at appreciable levels (Supplementary Figure 1C). Interestingly, expression of *Fos* was diffuse across all lung Treg clusters while expression of *Maf* was

enriched in cluster 3. To directly compare Tregs from lung and skin for GATA3- and T_H2-related gene expression, we performed combined clustering (Figure 1H). Skin and lung Tregs primarily clustered based on their tissue of origin (Figure 1H). Compared to lung, *Gata3* and *Irf4* expression were enriched in skin Tregs (Figure 1J). In addition, several of the GATA3-regulated genes (including *Areg*, *Maf*, *Il1rl1*, *Ero1l* and *Nfkbiz*) were preferentially expressed in skin Tregs, whereas Fos was expressed at similar levels in both skin and lung Tregs (Figure 1J and Supplementary Figure 1D). Additionally, several T_H2 associated cytokine and chemokine receptor genes were preferentially enriched in skin Tregs when compared to lung Tregs (Supplementary Figure 2).

Our bulk and single cell transcriptional analysis revealed *Gata3* to be highly expressed in skin Tregs. To validate this expression at the protein level we quantified GATA3 expression in Tregs isolated from skin, SDLNs and lung by flow cytometry. Consistent with our RNAseq data, Tregs in skin expressed high levels of GATA3 compared to SDLN and lung Tregs (Figure 1K). Taken together, these results suggest that Tregs in murine skin are preferentially 'T_H2 skewed', that this differentiation program is driven, at least in part, by GATA3 and that these cells may be more poised to regulate T_H2 immune responses relative to Tregs in lung.

Treg depletion results in increased T_H2 cytokine production in skin

Tregs express transcription factors and chemokine receptors that overlap with those of the effector cells that they are most poised to suppress, without expressing appreciable levels of the respective effector cytokines (20, 31–33). Transcription factor analysis of T effector cells ($CD4^+$, $Foxp3^-$) revealed that T_H2 cells were enriched in skin compared to lung (Supplementary figure 3). Because Tregs in skin are predominately T_H2 skewed, we asked whether these cells were most poised to suppress type 2 immune responses in this tissue. Diphtheria toxin (DT) was administered to $Foxp3^{DTR}$ mice (34) to deplete Tregs and 5 days later cytokine production from skin and lung $CD4^+$ T cells was quantified by flow cytometry. In these experiments, equivalent levels of Treg depletion was observed in skin and lung (Supplementary Figure 4A). Interestingly, Treg depletion resulted in a significantly increased accumulation of IL-13- and IL-4-producing T_H2 cells in skin with no appreciable increase in IFN-γ-producing T_H1 cells or IL-17 producing T_H17 cells (Figure 2A). In contrast, Treg depletion resulted in modest increases in T_H1, T_H2 and T_H17 cells in lung during the same 5-day time period (Figure 1A). In lung, increases in T_H1 and T_H17 cells were greater than increases in T_H2 cells after Treg depletion (Figure 2A). Of note, no statistically significant differences were observed in myeloid cell populations (*i.e.,* neutrophils, eosinophils, monocytes and inflammatory macrophages) in either skin or lung of Treg-depleted mice in this 5-day time period (Supplementary Figure 4B-E). Flow cytometric staining for intracellular cytokines is limited to quantifying cytokine production from T cells. Thus, we wanted to take a more holistic approach to determine how Treg depletion influenced cytokine gene expression at the whole tissue level. To do so, we treated $Foxp3^{DTR}$ mice or wildtype control mice with DT for 7 days and harvested RNA from full thickness dorsal skin and whole lung tissue for Qiagen cytokine qPCR array analysis. Treg depletion resulted in increased expression of RNA for several cytokines; however, there was a striking preferential increase in *Il13* expression (>20 $\log^2$-fold change) in skin when

compared to all other cytokines (Figure 2B). Heightened *Il13* expression was not observed in lung tissue (Figure 2B). Thus, both at the protein level in T cells and at the RNA level in whole tissue, our results suggest that Tregs preferentially regulate T_H2 immune responses (particularly IL-13) in skin in the steady state.

Acute depletion of Tregs results in dermal fibroblast activation and profibrotic gene expression in skin

An emerging body of literature suggests that qualitative and/or quantitative defects in Tregs are associated with chronic tissue fibrosing diseases such as hepatic fibrosis (35) and systemic sclerosis (36–39) (reviewed in(40)). Given that Tregs in skin preferentially attenuate T_H2 responses and T_H2 cytokines, such as IL-4 and IL-13, have been implicated in the pathogenesis of tissue fibrosis (3, 4), we hypothesized that Tregs in skin play a major role in regulating dermal fibroblast activation. To test this, we crossed αSMA-RFP reporter mice (41) to the FoxP3^{DTR} strain (34). The resultant αSMA-RFP/ FoxP3^{DTR} mice have red fluorescent protein (*RFP*) expressed under the control of the alpha smooth muscle actin (αSMA) promoter, a promoter that is highly active in profibrogenic myofibroblasts (42, 43). Tregs were depleted in these mice and αSMA-expressing dermal myofibroblasts were quantified by histology and flow cytometry (Figure 3A). Consistent with our hypothesis, we observed an increase in αSMA-expressing dermal myofibroblasts with time after Treg depletion by immunohistochemistry (Figure 3B). Flow cytometric quantification of αSMA-expressing myofibroblasts in skin corroborated these results with ~5-fold increase in accumulation of these cells 5 days after depleting Tregs (Figure 3C and Supplementary Figure 5A). To comprehensively elucidate the role of Tregs in regulating fibroblast activation in the steady-state, we performed 96-gene qRT-PCR ‘fibrosis pathway’ arrays on whole skin tissue harvested from FoxP3^{DTR} mice and control mice 5 days after beginning DT treatment. Compared to WT mice, Treg-depleted mice had a marked increase in profibrotic genes with minimal changes in anti-fibrotic genes (Figure 3D). In addition, Treg depletion resulted in heightened expression of many genes in the TGF-β pathway (Figure 3D). Taken together, these results suggest that Tregs attenuate fibroblast activation and fibrosis-associated gene expression in skin in the steady-state.

Chronic reduction of Tregs results in skin fibrosis

In the Treg depletion experiments described above (Figure 3), Tregs were completely ablated in an attempt to definitively establish their role in regulating fibroblast activation in skin. Because mice completely devoid of Tregs succumb to multi-organ autoimmunity ~15–20 days post Treg depletion (34), they do not live long enough to develop tissue fibrosis. Thus, we set out to determine if chronic reduction of Tregs results in persistent fibroblast activation and skin fibrosis. To do so, we took advantage of the fact that FoxP3 is expressed on the X-chromosome (44). Because FoxP3^{DTR} mice were generated by ‘knocking-in’ the DTR allele into the endogenous *FoxP3* locus (34), female mice that are heterozygous for the DTR allele (*i.e.,* FoxP3-DTR$^{+/-}$) have one copy of this transgene and one normal endogenous copy of *FoxP3*. Due to random X-chromosome inactivation, approximately 50% of Tregs in female FoxP3-DTR$^{+/-}$ mice are susceptible to DT-mediated deletion, while the remaining 50% are impervious to this treatment. To determine if Tregs could be chronically reduced in this model, we treated female FoxP3-DTR$^{+/-}$ mice or WT mice with DT 3x/week

for 4 weeks and quantified the percentages and absolute numbers of Tregs in skin and SDLNs. Female FoxP3-DTR$^{+/-}$ mice treated with DT showed a ~50% reduction in Tregs in skin (Supplementary Figure 6A. To determine if chronic reduction of Tregs results in fibroblast activation and skin fibrosis, we compared the dorsal skin of female αSMA-RFP/FoxP3-DTR$^{+/-}$ mice to female αSMA-RFP control mice 28 days after initiating DT treatment (Figure 4A). Consistent with our results after acute depletion of Tregs, chronic reduction of Tregs in αSMA-RFP/FoxP3-DTR$^{+/-}$ mice resulted in a significant accumulation of αSMA-expressing dermal myofibroblasts as quantified by flow cytometry (Figure 4B) and immunohistochemistry (Figure 4C). In addition, chronic Treg reduction resulted in increased dermal collagen density (Figure 4D) and significantly increased dermal thickening, with a significant reduction in subcutaneous dermal adipose tissue (Figure 4E). Quantitative RT-PCR fibrosis pathway analysis showed a very similar pattern to that observed in experiments where Tregs were completely depleted in the acute setting, with increased expression of profibrotic genes and a reduction in antifibrotic genes (Figure 4F). In addition, chronic Treg reduction resulted in increased expression of several genes in the TGF-β pathway as well as IL-13 and IL-5 (Figure 4F). Taken together, these results further support a major role for Tregs in regulating dermal fibroblast activation and skin fibrosis in the steady-state.

Tregs attenuate bleomycin induced skin fibrosis

The experiments described above suggest a major role for Tregs in regulating fibroblast activation in skin in the absence of tissue injury or inciting stimuli. We hypothesized that Tregs mediate these effects indirectly by preferentially regulating T_H2 cytokine production in skin. T_H2 immune responses have been shown to play critical roles in driving bleomycin-induced skin fibrosis in mice (45–48). Thus, we set out to determine if Tregs play a role in attenuating fibrosis in this model. To do so, we utilized the Treg reduction approach in female αSMA-RFP/FoxP3-DTR$^{+/-}$ mice as described above (Figure 4). Female αSMA-RFP/FoxP3-DTR$^{+/-}$ mice were treated with daily subcutaneous injections of bleomycin and given DT every three days for 14 days to reduce Treg numbers but not completely deplete these cells (see above and Supplemental Figure 3A). As controls, female αSMA-RFP/FoxP3-DTR$^{+/-}$ mice were treated with bleomycin but not Treg depleted (*i.e.,* not treated with DT) and female αSMA-RFP mice were treated with DT but not given bleomycin. Compared to DT-treated αSMA-RFP mice, bleomycin-treated αSMA-RFP/FoxP3$^{DTR+/-}$ mice had significantly higher intensity of αSMA staining (Figure 5A), increased collagen density (Figure 5B), increased dermal thickening with reduced dermal fat (Figure 5C), with enhanced accumulation of αSMA-expressing myofibroblasts (Figure 5D). These results indicate that skin fibrosis is readily apparent after 14 days of bleomycin treatment and that DT treatment alone does not induce fibroblast activation or fibrosis. Consistent with results when Tregs were reduced in the steady-state, Treg reduction in bleomycin treated αSMA-RFP/FoxP3$^{DTR+/-}$ mice resulted in significantly augmented fibrosis, with increased αSMA expression, collagen density, dermal thickness and myofibroblast accumulation (Figure 5A-D). Taken together, these results indicate that Tregs play a role in attenuating bleomycin-induced skin fibrosis.

Treg expression of GATA3 plays a role in suppressing fibroblast activation and dermal fibrosis

GATA3 has been coined the master regulator of T_H2 differentiation (21). Skin Tregs preferentially express high levels of GATA3, and these Tregs are significantly enriched in genes regulated by this transcription factor (Figure 1). Thus, we hypothesized that expression of GATA3 is responsible for mediating the anti-fibrotic effects of Tregs in skin. To test this, we crossed FoxP3^{CreERT2} mice (17) with Gata3$^{fl/fl}$ (49) mice to generate FoxP3^{CreERT2}/Gata3$^{fl/fl}$ animals that have inducible and selective deletion of *Gata3* in Tregs after administration of tamoxifen. FoxP3^{CreERT2}/Gata3$^{fl/fl}$ mice were treated with tamoxifen every 3 days starting on the same day as the initiation of bleomycin treatment. As controls, FoxP3^{CreERT2} mice were treated with bleomycin and tamoxifen. In addition, in some experiments, FoxP3^{CreERT2}/Gata3$^{fl/fl}$ were left untreated (*i.e.,* were not given tamoxifen or bleomycin) to control for induction of fibrosis. Administration of tamoxifen and bleomycin in FoxP3^{CreERT2}/Gata3$^{fl/fl}$ mice resulted in a significant reduction of GATA3 in skin Tregs relative to controls (Figure 6A). Importantly, this relatively short-term deletion of *Gata3* in Tregs did not result in reduced Treg numbers in skin, SDLNs or lung (Figure 6B). In addition, deletion of *Gata3* in Tregs did not affect their activation and stability, as measured by the mean fluorescence intensity of FoxP3, CD25 and CTLA4 over the 14-day treatment period (Supplementary Figure 7A-C). Deletion of *Gata3* in Tregs resulted in a significant increase in the percentage of IL-13 and IL-4-producing T_H2 cells in skin, with no change in the percentage of IFN-γ-producing and IL-17 producing Teff cells (Figure 6C). There was also a trend towards increased IL-13 production from ILC2s in skin upon *Gata3* deletion in Tregs (Supplementary Figure 7D &E). Consistent with the differential expression of GATA3 between skin-resident and lung-resident Tregs (Figure 1I and Figure 1K), deletion of *Gata3* in Tregs resulted in an approximate 80% increase in the percentage of T_H2 cells (as defined by T_H2 cytokine production) in skin, with no increase in T_H2 cells observed in lung (Figure 6D). There was no difference in skin-infiltrating proinflammatory macrophages or neutrophils in mice deficient in *Gata3*-expressing Tregs compared to controls (Figure 6E and Supplemental Figure 8A). Consistent with an increase in T_H2 cells, FoxP3^{CreERT2}Gata3$^{fl/fl}$ mice treated with both tamoxifen and bleomycin had increased dermal fibroblast activation, as evidenced by significantly augmented αSMA-expressing myofibroblasts when compared to tamoxifen- and bleomycin-treated FoxP3^{CreERT2} control mice (Figure 6F). Collagen density and dermal thickness were also increased in these animals with a concomitant reduction in dermal adipose tissue (Figure 6G, H). Histologic examination of lung tissue harvested from these animals revealed no significant differences between any of the groups (Supplemental Figure 9). Taken together, these results suggest that GATA3 mediates a transcriptional program in Tregs that confers these cells with the ability to preferentially suppressing T_H2 immune responses, and in doing so, enables optimal regulation of dermal fibroblast activation and skin fibrosis.

We set out to determine whether suppression of T_H2 cytokines by skin Tregs plays a role in their ability to regulate fibroblast activation and suppress skin fibrosis. In these experiments, we used Foxp3^{CreERT2}Gata3$^{fl/fl}$ mice to acutely delete *Gata3* in Tregs in our bleomycin model and determined whether blocking of T_H2 cytokines was capable of reversing the enhanced skin fibrosis observed in these animals. To block T_H2 cytokines, we used an anti-

IL4Rα (anti-CD124) antibody, which blocks both IL-4 and IL-13 signaling (50, 51). Isotype or anti-CD124 antibody was given intraperitoneally every two days along with tamoxifen to delete *Gata3* in Tregs. Bleomycin was injected every other day intradermally for the duration of the study (14 days). In these experiments, we observed a partial but significant reduction in collagen density and dermal thickness in skin of mice receiving anti-CD124 antibody compared to isotype treated control animals (Supplemental Figure 10). Interestingly, we did not observe a reduction in αSMA staining. A possible explanation for lack of a complete rescue in collagen density and dermal thickness with no change in αSMA staining could be from incomplete neutralization of IL-4 and IL-13 signaling using this pharmacologic approach. In addition, factors other than IL-4 and IL-13 (*i.e.,* IL-5, IL-9 and/or IL-10) may be contributing to enhanced fibrosis when *Gata3* is deleted in Tregs. Nevertheless, these results indicate that suppression of T_H2 cytokines plays a role, at least in part, to the mechanisms by which GATA3-expressing Tregs regulate skin fibrosis.

DISCUSSION

In recent years, Tregs have emerged as a highly dynamic immune cell subset influencing the function of non-immune cells in tissues (12). Our data suggest that Tregs are important mediators of myofibroblast accumulation in skin and chronic reduction of Tregs predisposes to clinically evident fibrosis. Tregs control fibroblast activation in skin by adapting a unique transcriptional program, which enables them to suppress profibrotic immune responses. Co-opting Teff transcriptional pathways to suppress specific immune responses is consistent with the unique functions of Tregs in tissues (19) (20).

Multiple lines of evidence suggest that tissue Tregs not only prevent autoimmunity but are also actively involved tissue in maintenance and repair (11, 12, 15). It has been shown previously that Tregs in skin and adipose tissue adopt a "T_H2 phenotype" which is identified by the expression of *Il1rl1* (ST2; IL-33 receptor) and *Areg*. (30). Our data supports these findings and expands on them, suggesting that although the majority of Tregs in skin express *Gata3*, *Areg* and *Il1rl1* are preferentially expressed on specific subsets (Figure 1). This expression pattern is quite different than that observed in lung-resident Tregs. Overall, our results suggest that Tregs in murine skin as an entire population are poised to regulate T_H2 immunity, and perhaps a subset of these cells are more differentiated towards having tissue reparative capacity.

The role of Tregs in fibrosis has been controversial due to several conflicting reports about their relative accumulation in fibrotic tissues and their ability to produce the profibrotic cytokine TGF-β (39) (52). It has been suggested that unstable Tregs accumulate in fibrotic tissues where they transdifferentiate into pathogenic T_H2/T_H17 cells (37). However, these studies did not go beyond correlating Treg frequencies with inflammatory disease. The ontogeny and functional capacity of these cells remain to be elucidated. Although Tregs have been shown to make TGF-β in specific contexts, they produce less of this cytokine in skin based on our RNAseq analysis. However, skin Tregs do express relatively high levels of several TGF-β receptors (10). Thus, we speculate that skin-resident Tregs could function as 'TGF-β sinks', acting to sequester this cytokine. In doing so, they would both prevent free

TGF-β from activating fibroblasts and may utilize this cytokine to maintain and/or enhance their regulatory capacity.

In Tregs, *Gata3* partners with FoxP3 to form a positive feedback loop to increase transcription of Treg-related genes. *Gata3* expression is important for maintaining the stability of Tregs under inflammatory conditions by reinforcing Foxp3 expression in dividing Tregs (53). Tregs that lack *Gata3* expression have been shown to be unstable and have the capacity to make IL-17A (54). Interestingly, we did not observe increased IL-17A production from *Gata3*-deficient Tregs in our fibrosis studies, nor did we observe any change in Treg numbers. We also did not observe differences in expression levels of CD25, CTLA-4 or Foxp3 between control and *Gata3*-deficient Tregs (Supplementary Figure 5A-C). This suggests that deletion of *Gata3* in Tregs did not result in 'unstable' cells in our experiments. We speculate that this is most likely secondary to the inducible Cre-lox system used in our study, which deleted *Gata3* in Tregs for a relatively short period of time (~14 days). This time frame may be too short to observe the Treg instability seen in models where constitutive *Gata3* deletion occurs in Tregs throughout development and the entire lifespan of the animal. Nevertheless, our data support a model whereby Gata3 mediates a transcriptional program in Tregs that acts to attenuate type 2 immune responses in skin independent of the role it plays in Treg stability.

Our findings suggest that quantitative or qualitative defects in Tregs may predispose to initiation of the fibrotic cascade. We show that these cells utilize a distinct transcriptional program to regulate fibrosis in skin. However, this is most likely only one of many mechanisms utilized by Tregs, including acting as 'TGF-β sinks', secretion of IL-10, and/or possibly direct interactions with fibroblasts to attenuate their activity. Further studies are required to discern the potential and relative roles of these and other pathways that Tregs utilize to control fibroblast activation. Given the differences in Tregs resident in healthy skin and lung shown here, it is possible that these cells utilize different mechanisms to regulate fibroblasts depending on the tissue. When compared to lung-resident Tregs, Tregs in skin preferentially express *Gata3* (Figure 1). Thus, we speculate that Treg control of profibrotic T_H2 responses is relatively skin-specific, or Tregs in lungs utilize a different mechanism to regulate T_H2 immunity. Recently, reduced Tregs in the liver have been implicated the pathogenesis of IL-22-mediated fibrosis of this organ (35), underscoring the idea that these cells most likely possess multiple mechanisms to attenuate fibrosis in a tissue dependent manner.

In conclusion, our study underscores the role of the regulatory arm of the immune system in the control of fibroblast activation and tissue fibrosis. Our results suggest that treatment modalities focused on augmenting the function of Tregs in skin may have profound effects in treating fibrosis in this organ. In addition, in contrast to targeting a single antifibrotic or profibrotic pathway, we speculate that augmenting cell types that naturally suppress fibrosis will capitalize on the multiple mechanisms utilized by these cells to mediate their anti-fibrotic effects.

MATERIALS AND METHODS

Mice.

Wild type C57BL/6, FoxP3^{GFP}, FoxP3^{DTR}, αSMA-RFP, FoxP3^{YFPCre} and FoxP3^{CreERT2} mice were purchased from The Jackson Laboratory. FoxP3^{DTR} mice (34) were crossed to αSMA-RFP mice (41) in house to generate FoxP3^{DTR}/αSMA-RFP mice. Gata3$^{fl/fl}$ (49) mice were a gift from Dr. Zena Werb at University of California, San Francisco. We crossed FoxP3^{CreERT2} mice (17) to Gata3$^{fl/fl}$ mice to generate FoxP3^{CreERT2}/ Gata3$^{fl/fl}$ mice in our mouse facility. Animal experiments were performed on 7- to 12-week-old mice. Mice were maintained through routine breeding at the University of California San Francisco (UCSF) School of Medicine in a specific pathogen free facility. All animal experiments were performed in accordance with guidelines established by Laboratory Animal Resource Center (LARC) at UCSF. All experimental plans and protocols were approved by IACUC beforehand.

Administration of diphtheria toxin, bleomycin, anti-CD124 antibody and tamoxifen.

Tregs were depleted from FoxP3^{DTR} mice by i.p. injection of DT (30) (50 mg/kg body weight; Sigma-Aldrich) every other day for 5 days (3 injections). Tregs were reduced from FoxP3$^{DTR+/-}$ mice by i.p. injection of DT (30 mg/kg body weight; Sigma-Aldrich) three times per week for 4 weeks (12 injections). Tissues were harvested on the indicated days as described in Results. Mice were compared to age- and gender-matched DT-treated WT mice or non-DT-treated littermates. In experiments using FoxP3^{CreERT2}/Gata3$^{fl/fl}$ mice, Cre recombinase was activated with tamoxifen (Sigma-Aldrich; 2.5 mg i.p. dissolved in corn oil) every 2 days for 14 days starting with concomitant injections of bleomycin (day 0). Mice were treated with bleomycin (Teva, NDC# 00703–3154-01) dissolved in PBS (1 unit/ml) every day for 14 days subcutaneously starting on day 0. In certain experiments, mice were treated with 100μg of anti-CD124 (anti-IL-4Rα) antibody (BD Pharmingen, Clone mIL4R-M1) or isotype (IgG2a, BD Pharmingen, Clone R-35–95) every 2 days for 14 days starting on day 0.

Cell preparation from tissues and stimulation for intracellular cytokine staining.

Single-cell suspensions of SDLNs were mechanically dissociated through a 100 μm filter and 2.5 cm^2 dorsal skin was processed as previously described (55). Single cells were washed in tissue culture media and filtered. Cells were counted using an automated cell counter (NucleoCounter NC 200; Chemomtec) to determine the absolute number of specific cell populations in skin by flow cytometry. 3–4 × 10^6 single cells were stained for flow cytometry or cultured for intracellular cytokine staining using a PMA & ionomycin cell stimulation cocktail (Tonbo Biosciences).

Flow cytometry.

Single-cell suspensions prepared above were pelleted and incubated with anti CD16/anti-CD32 (BD Biosciences; 2.4G2) in PBS. Cells were washed and stained with Ghost Viability dye (Tonbo Biosciences) in PBS. Following a wash in PBS, cells were stained for surface markers in PBS. For intracellular staining, cells were fixed and permeabilized with a FoxP3

buffer set (eBiosciences). Samples were run on a Fortessa analyzer (BD Biosciences) in the UCSF Flow Cytometry Core and collected using FACS Diva software (BD Biosciences). Flow cytometry data were analyzed using FlowJo software (Treestar). Fluorophore-conjugated antibodies specific for mouse surface and intracellular antigens were purchased from eBiosciences, BD Biosciences and Biolegend. The following antibodies and clones were used: anti-Ly6G (1A8), anti-CD11b (M1/70), anti-CD11c (HL3), anti-MHC Class II, (M5/114.15.2), anti-Ly6C (HK1.4), anti-IL-17 (TCA11–18H10.1), anti-IL-4 (11B11), anti-IL-13 (eBio13a), anti-IFN-γ (XMG1.2), anti-CD3 (145–2C11), anti-CD4 (RM4–5), anti-CD8 (SK1), anti-TCRγδ (GL3), anti-Gata3 (TWAJ), IL-10 (JES3), anti-CD45 (30-F11), and anti-FoxP3 (FJK-16s).

RNA sequencing analysis and qRT-PCR array.

For the analysis of fibrosis-related genes and chemokines, a 3 mm skin biopsy from mouse back skin was homogenized in a tissue lyser (gentleMACS; Miltenyi Biotec). RNA was isolated with the RNeasy fibrous tissue kit (Qiagen) and used to synthesize cDNA with a first strand synthesis kit (Qiagen). A mouse chemokine and cytokine array (Qiagen, RT2 Profiler PCR Array PAMM150-Z) was used to detect cytokine genes from back skin of mice. A mouse fibrosis array array (Qiagen; RT2 Profiler PCR Array PAMM120-Z) was used in experiments to detect expression of fibrosis-related genes in skin. For RNAseq, Treg cells were isolated by gating on live $CD45^{+}CD3^{+}CD4^{+}CD8^{-}CD25^{hi}CD27^{hi}$ cells, which contained greater than 90% Foxp3-expressing Tregs, from SDLNs and skin. Sorted cell populations were flash frozen in liquid nitrogen and sent overnight on dry ice to Expression Analysis, Quintiles (Morrisville, NC). RNA samples were converted into cDNA libraries using the Illumina TruSeq Stranded mRNA sample preparation kit (Illumina). RNA was isolated for expression analysis using QIAGEN RNeasy Spin Column and was quantified via Nanodrop ND-8000 spectrophotometer. RNA quality was checked by Agilent Bioanalyzer Pico Chip. cDNA was created from 220 pg of input RNA with the SMARTer Ultra Low input kit and sequenced to a 25M read depth with Illumina RNASeq. Reads were aligned to Ensembl mg GRCm38.p4 reference genome with TopHat software (v. 2.0.12). SAM files were generated with SAMtools from alignment results. Read counts were obtained with htseq-count (0.6.1p1) with the union option. Differential expression was determined using the R/Bioconductor package DESeq2 (Ref 2). Differentially expressed genes between skin Tregs and SDLN Tregs were analyzed by Ingenuity Pathway Analysis. To assess GATA3-regulated genes in Tregs, a curated gene list was generated from published dataset (26) and Gene Set Enrichment Analysis was performed (25).

Single cell RNA sequencing (scRNAseq).

Skin Tregs were prepared for scRNAseq by harvesting back skin from four C57BL/6 $FoxP3^{GFP}$ female adult mice. Back skin was harvested, digested, and processed as detailed above. Flow cytometry was performed on the post-digested single cell suspension and Ghost dye- CD45+ CD3+ CD4+ GFP+ cells were sorted to high purity.

Droplet-based single cell RNA sequencing.

Immediately post-sorting, Ghost dye^{-} $CD45^{+}$ $CD3^{+}$ $CD4^{+}$ GFP^{+} skin cells were run on the 10X Chromium (10X Genomics (27)) platform and library preparation was performed by

the Institute for Human Genetics at UCSF following the recommended protocol for the Chromium Single Cell 3' Reagent Kit (v2 Chemistry). Libraries were run on the HiSeq400 for Illumina sequencing. Post-processing and quality control were performed by the Genomics Core Facility in the Institute for Human Genomics at UCSF using the 10X Cell Ranger package (v1.2.0, 10X Genomics). Reads were aligned to mm10 reference assembly (v1.2.0, 10X Genomics). Primary assessment using this software showed 2,058 median unique molecular identifiers (UMIs, transcripts) per cell and 1,035 median genes per cell sequenced to 91.6% sequencing saturation with 88,229 mean reads per cell.

Unsupervised clustering of scRNAseq data.

The Seurat R package (version 2.2) (56) was used for graph-based clustering and visualizations. All functions mentioned are from the Seurat R package (version 2.2) or the standard R version 3.4.2 package and were used with default parameters unless otherwise noted. Cells (unique barcodes) that passed quality control processing and expressed at least 200 genes and only genes that were expressed in 3 or more cells were analyzed. Cells with greater than 10% mitochondrial genes and greater than 30% ribosomal protein genes were removed from downstream analysis.

Library-size normalization was applied to each cell with the NormalizeData function. Normalized expression for gene i in cell j was calculated by taking the natural log of the UMI counts for gene i in cell j divided by the total UMI counts in cell j multiplied by 10,000 and added to 1. To reduce the influence of variability in the number of UMIs, mitochondrial gene expression and ribosomal gene expression between cells on the clustering, we used the ScaleData function to linearly regress out these sources of variation before scaling and centering the data for dimensionality reduction. Principal component analysis was run using the RunPCA function on the variable genes calculated with the FindVariableGenes function. Based on the PCElbowPlot function result we decided to use 19 principle components (PCs) for clustering. We ran the FindClusters function to apply shared nearest neighbor (SNN) graph-based clustering (0.6 resolution) and used the FindAllMarkers function (Wilcoxon rank sum test, min.pct = 0.25, only.pos = True, thresh.use = 0.25) to identify small clusters of macrophages (*Cd68*+) and fibroblasts (*Col1a1*+) to be removed. The non-Treg cells may have been collected due to doublets and/or sorting impurity. The remaining cells in each sample were then normalized and scaled as above. Log-normalized gene expression data was used for visualizations with tSNE plots (FeaturePlot).

Gene Set Enrichment Analysis (GSEA).

We generated a preranked list of genes ranking relative expression of skin Tregs versus Tregs in SDLNs using DESeq2 and performed GseaPreranked analysis using the GSEA v3.0 tool with default settings (24, 25). Gene sets tested were described to be either positively (fold-change >= 2 in WT versus *Gata3*-deleted cells) or negatively (fold-change <= 0.5 in WT versus *Gata3*-deleted cells) regulated by *GATA3* in T_H1, T_H2, T_H17 and iTreg cells as described by (26).

Histology and immunofluorescence microscopy.

For histopathology, skin tissue was fixed in 10% formalin and paraffin-embedded. Tissue was stained with hematoxylin and eosin (H&E), Masson's Trichrome and anti-αSMA by the University of California San Francisco Mouse Pathology Core. H&E quantifications of epidermal hyperplasia, collagen density and αSMA intensity were performed using ImageJ64 software (NIH, USA). For quantification, 3–5 measurements per slide/sample for each mouse per group (n=3–7) were taken, with every measurement plotted and the average of all measurements shown.

Statistical Analyses.

Statistical analyses were performed with Prism software package version 7.0 (GraphPad). P values were calculated using two-tailed unpaired Student's t-test or one-way ANOVA. Pilot experiments were used to determine sample size for animal experiments. No animals were excluded from analysis, unless due to technical errors. Mice were age- and gender-matched and randomly assigned into experimental groups. Appropriate statistical analyses were applied, assuming a normal sample distribution. All in vivo mouse experiments were conducted with at least 2–3 independent animal cohorts. RNAseq experiments were conducted using 3–4 biological samples. Data are reported as mean ± S.E.M. P values correlate with symbols as follows: ns = not significant, $p>0.05$, *$p<0.05$, **$p<0.01$, ***$p<0.001$, ****$p<0.0001$.

Supplementary Material

Refer to Web version on PubMed Central for supplementary material.

ACKNOWLEDGEMENTS

We would like to thank the UCSF Parnassus Flow Cytometry Core which is supported by the Diabetes Research Center (DRC) grant NIH P30 DK063720 and the UCSF Mouse Pathology Core which is supported by NIH 5P30CA082103–15.

FUNDING

This work was primarily funded by M.D.R.'s Scleroderma Research Foundation (SRF) grant. Additional grant support was provided by M.D.R.'s NIH K08-AR062064, NIH DP2-AR068130, Pfizer ASPIRE Grant WI229090, NIH R01-AR071944, and L.A.K's Frontiers in Medical Research Fellowship from California Foundation of Molecular Biology and QB3. A.H. was supported by a Dermatology Foundation Career Development Award.

REFERENCES AND NOTES

1. Varga JA, Trojanowska M, Fibrosis in systemic sclerosis. Rheum. Dis. Clin. North Am 34, 115–43–vii (2008).
2. Wynn TA, Ramalingam TR, Mechanisms of fibrosis: therapeutic translation for fibrotic disease. Nature Medicine. 18, 1028–1040 (2012).
3. Lee CG et al., Interleukin-13 induces tissue fibrosis by selectively stimulating and activating transforming growth factor beta(1). J. Exp. Med 194, 809–821 (2001). [PubMed: 11560996]
4. Ramalingam TR et al., Unique functions of the type II interleukin 4 receptor identified in mice lacking the interleukin 13 receptor alpha1 chain. Nat. Immunol 9, 25–33 (2008). [PubMed: 18066066]

5. Chiaramonte MG et al., Regulation and function of the interleukin 13 receptor alpha 2 during a T helper cell type 2-dominant immune response. J. Exp. Med 197, 687–701 (2003). [PubMed: 12642601]
6. Meng X-M, Nikolic-Paterson DJ, Lan HY, TGF-β: the master regulator of fibrosis. Nat Rev Nephrol 12, 325–338 (2016). [PubMed: 27108839]
7. Sefik E et al., MUCOSAL IMMUNOLOGY. Individual intestinal symbionts induce a distinct population of RORγ$^+$ regulatory T cells. Science. 349, 993–997 (2015). [PubMed: 26272906]
8. Arpaia N et al., A Distinct Function of Regulatory T Cells in Tissue Protection. Cell. 162, 1078–1089 (2015). [PubMed: 26317471]
9. D'Alessio FR et al., CD4+CD25+Foxp3+ Tregs resolve experimental lung injury in mice and are present in humans with acute lung injury. J. Clin. Invest. 119, 2898–2913 (2009). [PubMed: 19770521]
10. Ali N, Rosenblum MD, Regulatory T cells in skin. Immunology. 152, 372–381 (2017). [PubMed: 28699278]
11. Ali N et al., Regulatory T Cells in Skin Facilitate Epithelial Stem Cell Differentiation. Cell. 169, 1119–1129.e11 (2017). [PubMed: 28552347]
12. Panduro M, Benoist C, Mathis D, Tissue Tregs. Annu. Rev. Immunol 34, 609–633 (2016). [PubMed: 27168246]
13. Burzyn D et al., A special population of regulatory T cells potentiates muscle repair. Cell. 155, 1282–1295 (2013). [PubMed: 24315098]
14. Bapat SP et al., Depletion of fat-resident Treg cells prevents age-associated insulin resistance. Nature. 528, 137–141 (2015). [PubMed: 26580014]
15. Mathur AN et al., Treg-Cell Control of a CXCL5-IL-17 Inflammatory Axis Promotes Hair-Follicle-Stem-Cell Differentiation During Skin-Barrier Repair. Immunity. 50, 655–667.e4 (2019). [PubMed: 30893588]
16. Josefowicz SZ et al., Extrathymically generated regulatory T cells control mucosal TH2 inflammation. Nature. 482, 395–399 (2012). [PubMed: 22318520]
17. Rubtsov YP et al., Regulatory T cell-derived interleukin-10 limits inflammation at environmental interfaces. Immunity. 28, 546–558 (2008). [PubMed: 18387831]
18. Worthington JJ et al., Integrin αvβ8-Mediated TGF-β Activation by Effector Regulatory T Cells Is Essential for Suppression of T-Cell-Mediated Inflammation. Immunity. 42, 903–915 (2015). [PubMed: 25979421]
19. Chaudhry A et al., Interleukin-10 signaling in regulatory T cells is required for suppression of Th17 cell-mediated inflammation. Immunity. 34, 566–578 (2011). [PubMed: 21511185]
20. Zheng Y et al., Regulatory T-cell suppressor program co-opts transcription factor IRF4 to control T(H)2 responses. Nature. 458, 351–356 (2009). [PubMed: 19182775]
21. Lin W et al., Regulatory T cell development in the absence of functional Foxp3. Nat. Immunol 8, 359–368 (2007). [PubMed: 17273171]
22. Zheng W, Flavell RA, The transcription factor GATA-3 is necessary and sufficient for Th2 cytokine gene expression in CD4 T cells. Cell. 89, 587–596 (1997). [PubMed: 9160750]
23. Rengarajan J et al., Interferon regulatory factor 4 (IRF4) interacts with NFATc2 to modulate interleukin 4 gene expression. J. Exp. Med 195, 1003–1012 (2002). [PubMed: 11956291]
24. Mootha VK et al., PGC-1alpha-responsive genes involved in oxidative phosphorylation are coordinately downregulated in human diabetes. Nat. Genet 34, 267–273 (2003). [PubMed: 12808457]
25. Subramanian A et al., Gene set enrichment analysis: a knowledge-based approach for interpreting genome-wide expression profiles. Proc. Natl. Acad. Sci. U.S.A. 102, 15545–15550 (2005). [PubMed: 16199517]
26. Wei G et al., Genome-wide analyses of transcription factor GATA3-mediated gene regulation in distinct T cell types. Immunity. 35, 299–311 (2011). [PubMed: 21867929]
27. Zheng GXY et al., Massively parallel digital transcriptional profiling of single cells. Nat Commun 8, 14049 (2017). [PubMed: 28091601]

28. Ivanov II et al., The orphan nuclear receptor RORgammat directs the differentiation program of proinflammatory IL-17+ T helper cells. Cell. 126, 1121–1133 (2006). [PubMed: 16990136]
29. Szabo SJ et al., A novel transcription factor, T-bet, directs Th1 lineage commitment. Cell. 100, 655–669 (2000). [PubMed: 10761931]
30. Delacher M et al., Genome-wide DNA-methylation landscape defines specialization of regulatory T cells in tissues. Nat. Immunol 18, 1160–1172 (2017). [PubMed: 28783152]
31. Chaudhry A et al., CD4+ regulatory T cells control TH17 responses in a Stat3-dependent manner. Science. 326, 986–991 (2009). [PubMed: 19797626]
32. Koch MA et al., The transcription factor T-bet controls regulatory T cell homeostasis and function during type 1 inflammation. Nat. Immunol 10, 595–602 (2009). [PubMed: 19412181]
33. Levine AG et al., Stability and function of regulatory T cells expressing the transcription factor T-bet. Nature. 546, 421–425 (2017). [PubMed: 28607488]
34. Kim JM, Rasmussen JP, Rudensky AY, Regulatory T cells prevent catastrophic autoimmunity throughout the lifespan of mice. Nat. Immunol 8, 191–197 (2007). [PubMed: 17136045]
35. Fabre T et al., Type 3 cytokines IL-17A and IL-22 drive TGF-β-dependent liver fibrosis. Sci Immunol 3, eaar7754 (2018).
36. Kataoka H et al., Decreased expression of Runx1 and lowered proportion of $Foxp3^{+}$ $CD25^{+}$ $CD4^{+}$ regulatory T cells in systemic sclerosis. Mod Rheumatol 25, 90–95 (2015). [PubMed: 24716598]
37. MacDonald KG et al., Regulatory T cells produce profibrotic cytokines in the skin of patients with systemic sclerosis. J. Allergy Clin. Immunol 135, 946–.e9 (2015). [PubMed: 25678090]
38. Antiga E et al., Regulatory T cells in the skin lesions and blood of patients with systemic sclerosis and morphoea. Br. J. Dermatol 162, 1056–1063 (2010). [PubMed: 20105169]
39. Klein S et al., Reduction of regulatory T cells in skin lesions but not in peripheral blood of patients with systemic scleroderma. Ann. Rheum. Dis 70, 1475–1481 (2011). [PubMed: 21097800]
40. Slobodin G, Rimar D, Regulatory T Cells in Systemic Sclerosis: a Comprehensive Review. Clin Rev Allergy Immunol 52, 194–201 (2017). [PubMed: 27318947]
41. LeBleu VS et al., Identification of human epididymis protein-4 as a fibroblast-derived mediator of fibrosis. Nature Medicine. 19, 227–231 (2013).
42. Hinz B, Celetta G, Tomasek JJ, Gabbiani G, Chaponnier C, Alpha-smooth muscle actin expression upregulates fibroblast contractile activity. Mol. Biol. Cell. 12, 2730–2741 (2001). [PubMed: 11553712]
43. Hinz B, Formation and function of the myofibroblast during tissue repair. J. Invest. Dermatol 127, 526–537 (2007). [PubMed: 17299435]
44. Hori S, Nomura T, Sakaguchi S, Control of regulatory T cell development by the transcription factor Foxp3. Science. 299, 1057–1061 (2003). [PubMed: 12522256]
45. Karo-Atar D et al., A protective role for IL-13 receptor α 1 in bleomycin-induced pulmonary injury and repair. Mucosal Immunol 9, 240–253 (2016). [PubMed: 26153764]
46. Wilson MS et al., Bleomycin and IL-1beta-mediated pulmonary fibrosis is IL-17A dependent. J. Exp. Med 207, 535–552 (2010). [PubMed: 20176803]
47. Cipolla E et al., IL-17A deficiency mitigates bleomycin-induced complement activation during lung fibrosis. FASEB J. 31, 5543–5556 (2017). [PubMed: 28821630]
48. Jakubzick C et al., Therapeutic attenuation of pulmonary fibrosis via targeting of IL-4-and IL-13-responsive cells. J. Immunol 171, 2684–2693 (2003). [PubMed: 12928422]
49. Pai S-Y et al., Critical roles for transcription factor GATA-3 in thymocyte development. Immunity. 19, 863–875 (2003). [PubMed: 14670303]
50. Andrews A-L, Holloway JW, Holgate ST, Davies DE, IL-4 receptor alpha is an important modulator of IL-4 and IL-13 receptor binding: implications for the development of therapeutic targets. J. Immunol 176, 7456–7461 (2006). [PubMed: 16751391]
51. Kasaian MT et al., An IL-4/IL-13 dual antagonist reduces lung inflammation, airway hyperresponsiveness, and IgE production in mice. Am. J. Respir. Cell Mol. Biol 49, 37–46 (2013). [PubMed: 23449738]
52. Birjandi SZ et al., CD4(+)CD25(hi)Foxp3(+) Cells Exacerbate Bleomycin-Induced Pulmonary Fibrosis. Am. J. Pathol 186, 2008–2020 (2016). [PubMed: 27317904]

53. Rudra D et al., Transcription factor Foxp3 and its protein partners form a complex regulatory network. Nat. Immunol 13, 1010–1019 (2012). [PubMed: 22922362]

54. Wohlfert EA et al., GATA3 controls Foxp3^{+} regulatory T cell fate during inflammation in mice. J. Clin. Invest 121, 4503–4515 (2011). [PubMed: 21965331]

55. Gratz IK et al., Cutting edge: Self-antigen controls the balance between effector and regulatory T cells in peripheral tissues. J. Immunol 192, 1351–1355 (2014). [PubMed: 24442443]

56. Butler A, Hoffman P, Smibert P, Papalexi E, Satija R, Integrating single-cell transcriptomic data across different conditions, technologies, and species. Nat. Biotechnol 36, 411–420 (2018). [PubMed: 29608179]

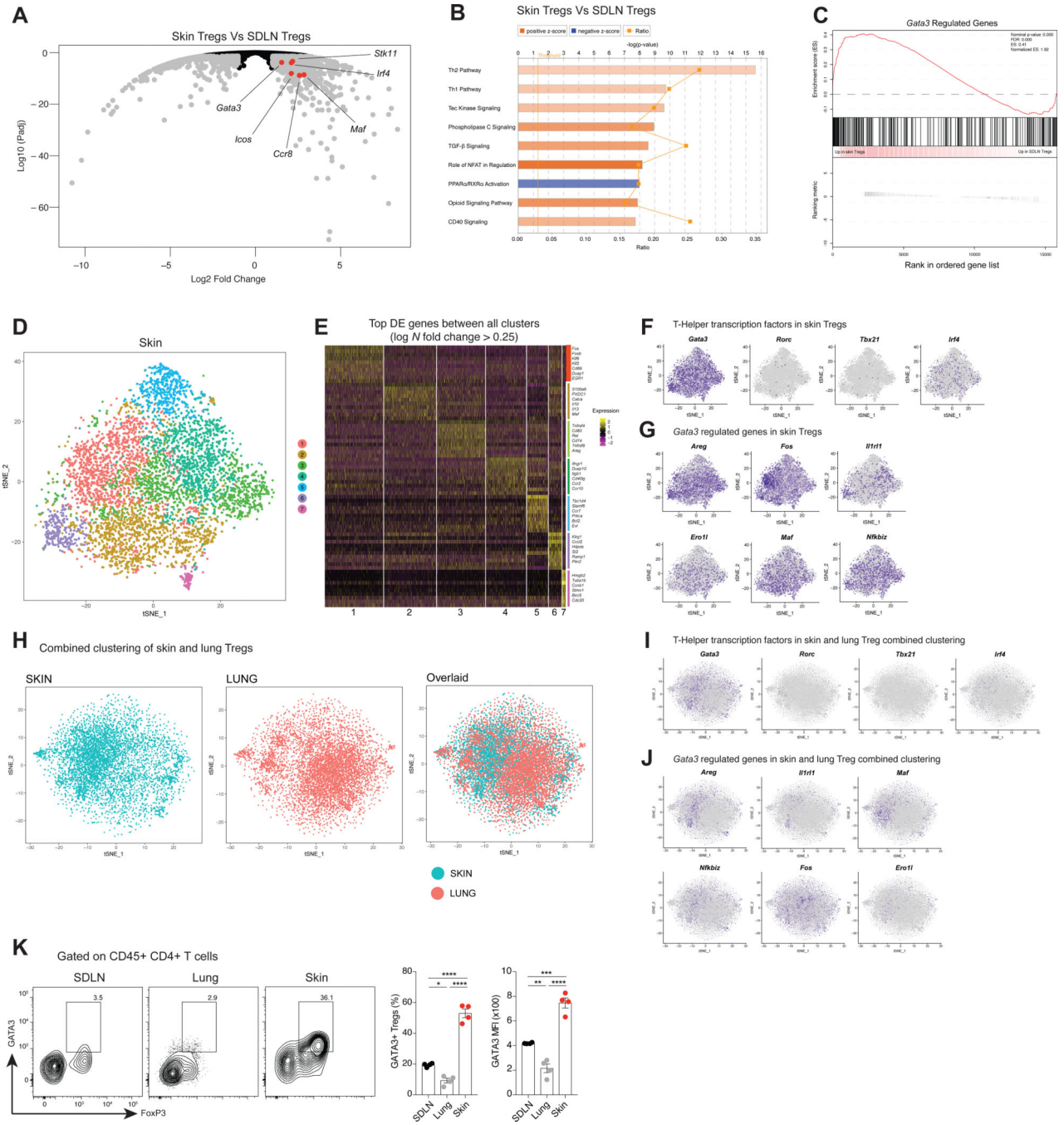

Figure 1. Bulk cell and single cell analysis of Tregs in murine skin reveals a skewing towards T_H2 differentiation.

(A-C) Foxp3-GFP$^+$CD25$^+$ Tregs were sorted from skin-draining lymph nodes (SDLNs) and skin of FoxP3^{GFP} reporter mice for whole transcriptome RNA sequencing. (**A**) Volcano plot comparing expression profiles of skin versus SDLN Tregs. (**B**) Inginuity Pathway Analysis of differentially expressed genes between skin and SDLN Tregs. (**C**) Gene set enrichment analysis of *Gata3* regulated genes in skin and SDLN Tregs. (D-G) Foxp3-GFP$^+$CD25$^+$ Tregs were sort purified from skin of FoxP3^{GFP} reporter mice for single cell RNA sequencing

using the 10xGenomics platform. (**D**) t-SNE plot of skin Tregs. (**E**) Heat map with genes enriched in each skin Treg cluster (**F**) Feature plot of specific transcription factors and (**G**) genes regulated by *Gata3*. (**H**) Combined clustering t-SNE plot of skin and lung Tregs (**I**) Feature plot of specific transcription factors and (**J**) genes regulated by *Gata3* in combined t-SNE plot of skin and lung Tregs (**K**) Representative contour plots and flow cytometric quantification of GATA3 expression in Tregs isolated from SDLNs, skin and lungs of healthy wildtype mice. Cells are pre-gated on Live $CD45^+CD3^+CD4^+$ T cells. MFI, mean fluorescence intensity. Data are representative of 3 independent experiments, n=3–5 mice per group, per experiment. Data are ± Standard Error Mean (SEM). One-way ANOVA *p<0.05, **p<0.01, ***p<0.001, ****p<0.0001, ns=not significant.

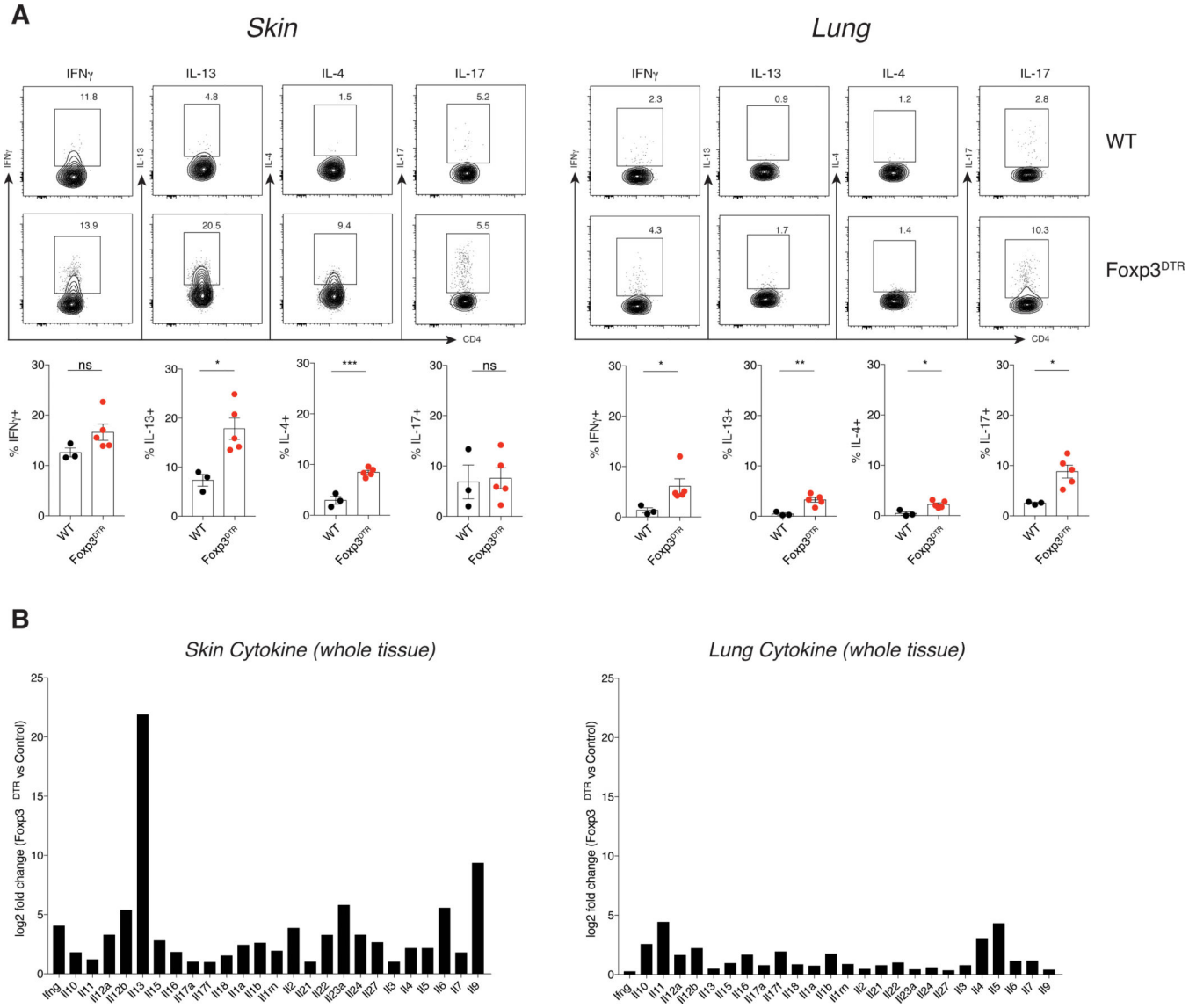

Figure 2. Tregs preferentially regulate T_H2 cytokines in skin.

C57/B6 (WT) or FoxP3$^{DTR+/+}$ (FoxP3^{DTR}) mice (homozygous for the Foxp3^{DTR} transgene) were treated with diphtheria toxin (DT) every 2 days and skin and lung tissue harvested on day 5. Cells from skin and lung from WT (black circles) and Foxp3^{DTR} mice (red circles) were stimulated with PMA/Ionomycin and intracellular cytokine production quantified by flow cytometry. (**A**) Representative flow cytometric plot for each cytokine tested and quantification shown below. (**B**) Quantitative RT-qPCR for cytokine genes using Qiagen RT^2 Profiler Arrays on mRNA isolated from whole skin or lung of WT or Foxp3^{DTR} mice 7 days after beginning treatment with DT with three replicates each. Log_2-fold change in expression levels of cytokine genes with a statistical significance of $p<0.05$ is shown.

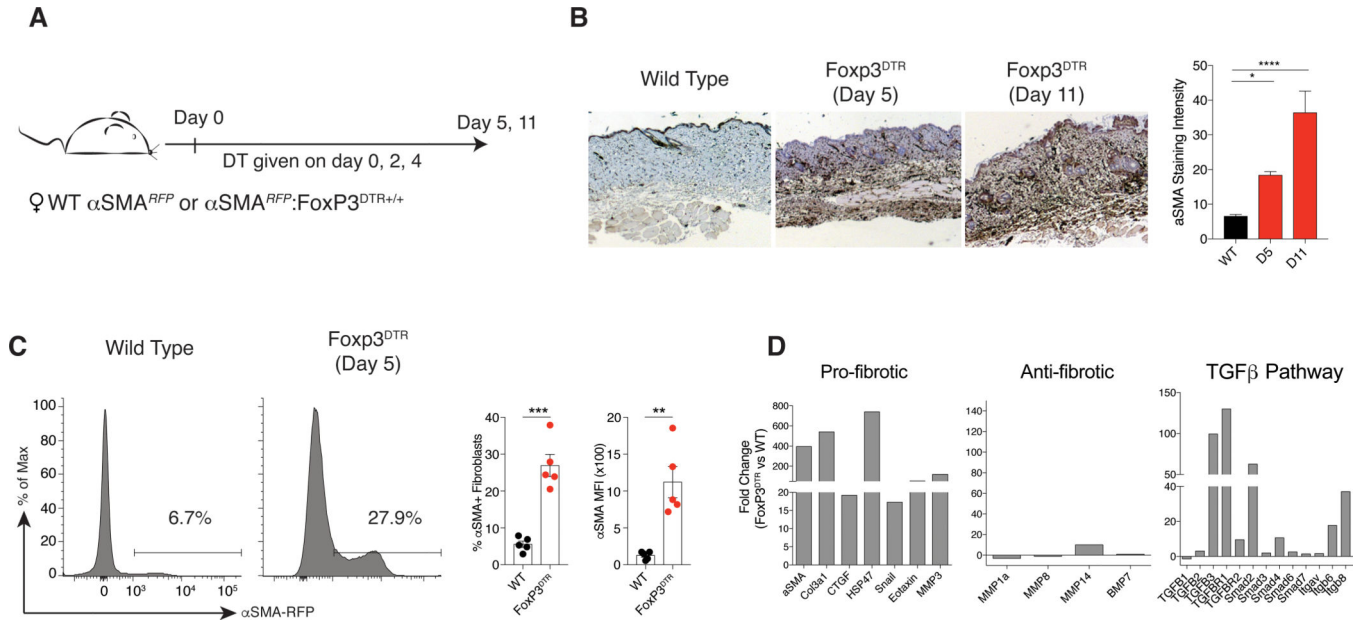

Figure 3. Tregs regulate fibroblast activation and profibrotic gene expression in skin.

(**A**) αSMA-RFP mice (WT) or FoxP3$^{DTR+/+}$/αSMA-RFP (FoxP3^{DTR}) mice (homozygous for the Foxp3^{DTR} transgene) were treated with diphtheria toxin (DT) every 2 days and skin was harvested on day 5. (**B**) Representative αSMA staining of dorsal skin tissue sections on day 5, 11 after DT treatment and quantification of αSMA staining intensity. (**C**) Representative histograms and flow cytometric quantification of αSMA expression on dermal fibroblasts (Live CD45^{-}PDPN^{+}PDGFRα^{+} cells) after Treg depletion on day 5. (**D**) Quantitative RT-qPCR for fibrosis associated genes using Qiagen RT^{2} Profiler Array on mRNA isolated from whole skin of WT or Foxp3^{DTR} mice on day 5 (n=3). Fold change in expression levels of profibrotic, antifibrotic, and TGF-β pathway is shown. Unpaired t-test, *p<0.05 **p<0.01, ***p<0.001, ****p<0.0001, ns=not significant.

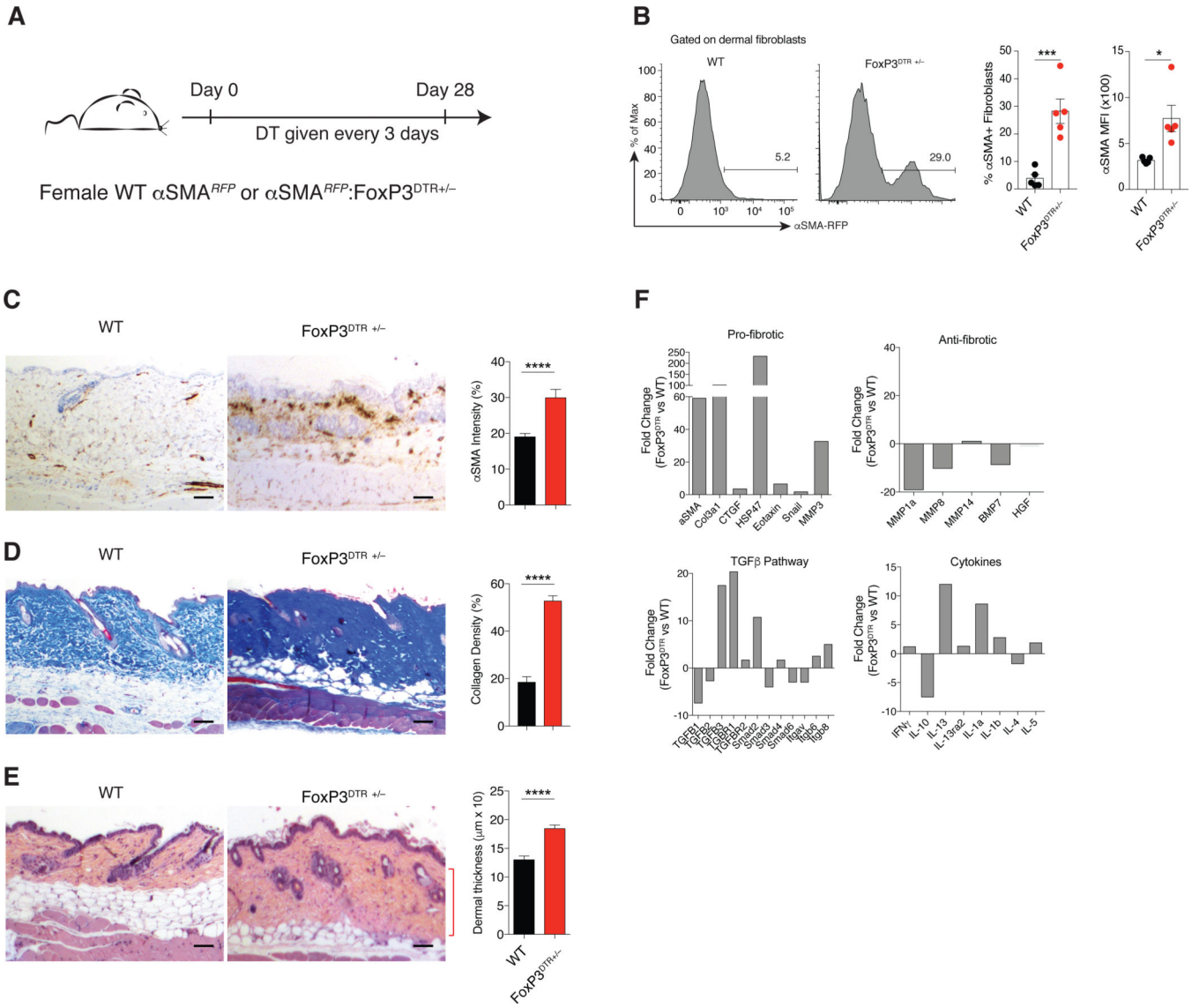

Figure 4. Chronic Treg reduction results in dermal fibrosis.

(**A**) αSMA-RFP mice (WT) or FoxP3$^{DTR-/+}$/αSMA-RFP (FoxP3$^{DTR-/+}$) mice (heterozygous for the Foxp3^{DTR} transgene) were treated with diphtheria toxin (DT) every 3 days and skin has harvested on day 28. (**B**) Representative histograms and flow cytometric quantification of αSMA expression on dermal fibroblasts on day 28. (**C**) Representative αSMA staining of dorsal skin tissue sections on day 28 after DT treatment and quantification of αSMA staining intensity. (**D**) Representative Masson's trichrome staining of dorsal skin tissue sections and quantification of collagen density. **(E)** Representative Hematoxylin and eosin (H&E) stain and quantification of dermal thickness indicated by red line on the image. (**F**) Quantitative RT-qPCR for fibrosis associated genes on mRNA isolated from whole skin of WT or Foxp3$^{DTR-/+}$ mice on day 28. Fold change in expression levels of profibrotic, antifibrotic, TGF-β pathway and cytokine genes is shown. All data are representative of 3 independent experiments, n=5 mice per group, per experiment. Data are

± Standard Error Mean (SEM). Unpaired t-test, *p<0.05 **p<0.01, ***p<0.001, ****p<0.0001, ns=not significant. Scale bar = 100μm.

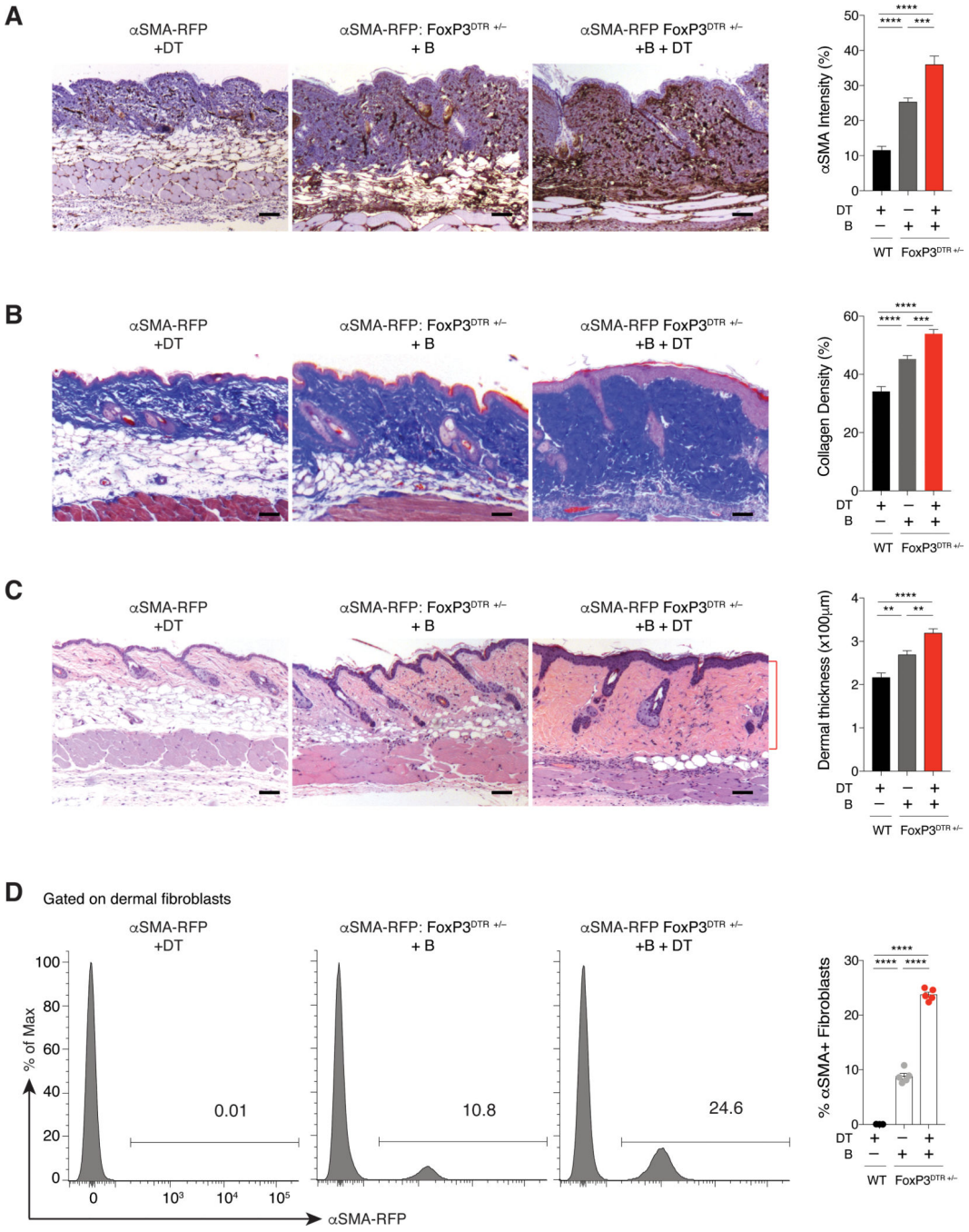

Figure 5. Chronic Treg reduction exacerbates bleomycin-induced skin fibrosis.

αSMA-RFP: FoxP3$^{DTR+/-}$ mice (heterozygous for the Foxp3^{DTR} transgene) were treated with either bleomycin only or with bleomycin and DT for 14 days. αSMA-RFP mice treated with DT were used as baseline controls. (**A**) Representative αSMA staining of dorsal skin on day 14 and histologic quantification of αSMA staining intensity from control (αSMA-RFP + DT, black circles), αSMA-RFP: FoxP3$^{DTR+/-}$ treated with bleomycin alone (grey circles) and αSMA-RFP: FoxP3$^{DTR+/-}$ treated with bleomycin and DT (red circles), B=bleomycin. (**B**): Representative Masson's trichrome staining of dorsal skin on day 14 and

histologic quantification of collagen density. (**C**) Representative Hematoxylin and eosin (H&E) stain on day 14 and quantification of dermal thickness. (**D**) Representative histograms and flow cytometric quantification of αSMA expression on dermal fibroblasts after Treg reduction. Data are representative of 3 independent experiments, n=3–5 per group, per experiment. Data are ± Standard Error Mean (SEM). One-way ANOVA **p<0.01, ***p<0.001, ****p<0.0001, ns=not significant. Scale bar = 100μm

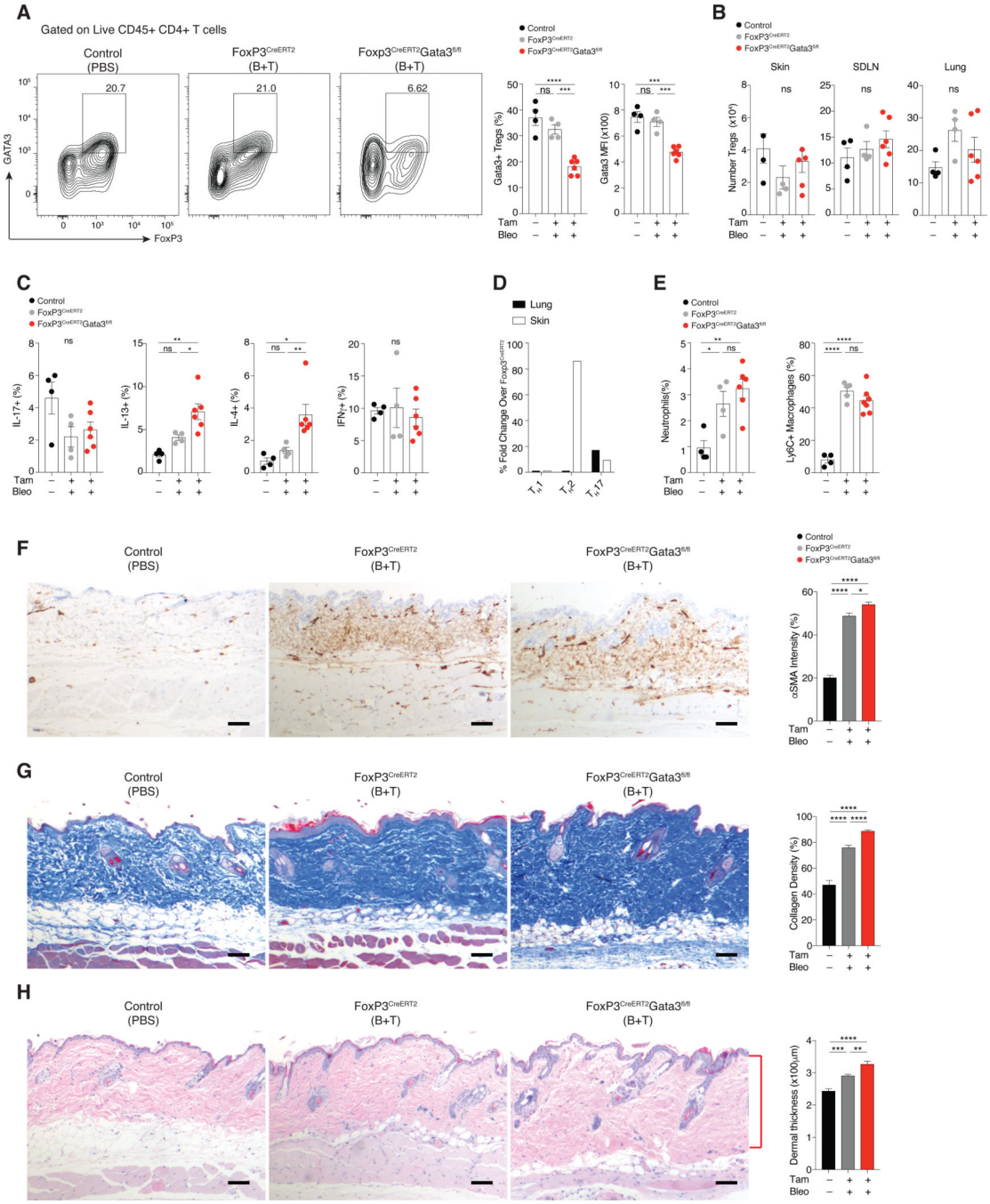

Figure 6. Treg expression of Gata3 plays a major role in controlling dermal fibrosis.

FoxP3^{CreERT2} or FoxP3^{CreERT2}/Gata3$^{fl/fl}$ mice were treated with bleomycin (B) and tamoxifen (T) for 14 days. FoxP3^{CreERT2}/Gata3$^{fl/fl}$ treated with PBS (no bleomycin or tamoxifen) were used as baseline controls. (**A)** Representative contour plots and flow cytometric quantification of GATA3 expression in skin CD4+ T cells on day 14. (**B)** Flow cytometric quantification of Tregs (Live CD45^{+}CD4^{+}FoxP3^{+} cells) isolated from skin, SDLNs and lungs on day 14. (**C**) Flow cytometric quantification of percent of cytokine (IL-17, IL-13, IL-4, and IFN-γ) producing Teff cells (live CD45^{+}CD4^{+}FoxP3^{-}) after PMA/

Ionomycin stimulation for 4 hrs from skin. (**D**) Fold change in the percentage of CD4+ helper T cell (T_H) subsets from skin and lung of bleomycin and tamoxifen treated FoxP3^{CreERT2}/Gata3$^{fl/fl}$ mice versus FoxP3^{CreERT2} mice. (**E**) Percentage of neutrophils (CD45$^+$MHCII$^-$Ly6G$^+$) and inflammatory macrophages (CD45$^+$MHCII$^+$CD11b$^+$F4/80$^+$Ly6C$^+$). **(F)** Representative αSMA tissue staining of dorsal skin and histologic quantification of αSMA staining intensity on day 14. (**G**) Representative Masson's trichrome staining and histologic quantification of collagen density. (**H**) Representative Hematoxylin and Eosin (H&E) staining and quantification of dermal thickness. MFI, mean fluorescence intensity. Data are representative of 2 independent experiments, n=4–7 per group, per experiment. Data are ± Standard Error Mean (SEM). One-way ANOVA *p<0.05 **p<0.01, ***p<0.001, ****p<0.0001, ns=not significant. Scale bar = 100μm